Icarus 409 (2024) 115870

Contents lists available at ScienceDirect

Icarus

journal homepage: www.elsevier.com/locate/icarus

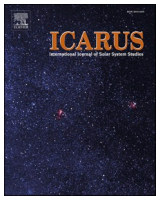

Search for carbonaceous chondrites evidence on Vesta through the detection of carbonates

G. Massa [a,b,*], E. Palomba [a], A. Longobardo [a], M. Angrisani [a,b], C. Gisellu [a,b], F. Dirri [a], M.C. De Sanctis [a], A. Raponi [a], F.G. Carrozzo [a], M. Ciarniello [a]

[a] INAF Istituto di Astrofisica e Planetologia Spaziali, via Fosso del Cavaliere, Rome 00133, Italy
[b] University of Rome "Sapienza", Piazzale Aldo Moro 5, Rome 00185, Italy

ARTICLE INFO

Keywords:
Asteroid
Spectroscopy
Surface
Vesta
Carbonaceous chondrites

ABSTRACT

NASA's Dawn mission was launched in September 2007 and orbited asteroids Vesta (2011−2012) and Ceres (2015–2018). Vesta shows surface dark units that have been suggested to be linked to exogenous materials and are therefore useful to understand the initial stages of the Solar System.

This work takes advantage of the newly calibrated data of the VIR spectrometer, which are characterized by a better signal to noise (S/N) ratio, giving us the opportunity to search for spectral features that were never seen before due to noise. Considering that hydroxyl has been shown to be present in every dark unit on Vesta and also in carbonaceous chondrites, the goals of this work are the search for and characterization of carbonates that are present in carbonaceous chondrites, i.e., the supposed darkening agents of Vesta.

The estimate of the abundances of carbonates is fundamental to identify which carbonaceous chondrite fell on Vesta; this can be crucial for the definition of an evolutionary history of Vesta and the Solar System. The study of a possible feature at 3.9 μm related to the presence of carbonates was analyzed and found to be noise-induced. Although spectral features related to carbonates were not observed, the 3.4 μm absorption band was analyzed anyway in order to fix an upper limit to the abundance of carbonates in carbonaceous chondrites on Vesta. This value is consistent with petrochemical analyses, i.e., no more than 0.2% of carbonates in carbonaceous chondrites.

1. Introduction

The Dawn spacecraft's scientific payload consisted of a Framing Camera (FC) (Sierks et al., 2011), a Visible and InfraRed spectrometer (VIR) (De Sanctis et al., 2011) and a Gamma Ray and Neutron Detector (GRaND) (Prettyman et al., 2011), as well as a radio science experiment.

The asteroid 4 Vesta is a differentiated asteroid, i.e., it has experienced melting and now its structure is composed of distinct layers: crust, mantle, and core. Hence, studying the materials coming from different depths of Vesta could be helpful to understand its evolutionary history. It also preserves information on the composition of smaller primordial asteroids that impacted its surface.

Prior to Dawn's arrival in 2011, all information about Vesta was derived from telescopic observations. Also, an increasing number of small asteroids with a similar surface composition were discovered and taxonomically classified as V-type asteroids (DeMeo et al., 2009). Most of them can be linked to Vesta instead of other asteroids that do not appear to have a clear link to Vesta, suggesting the existence of other basaltic parent bodies (Xu et al., 1995; Duffard et al., 2004; Alvarez-Candal et al., 2006). The reflectance spectra of Vesta and V-type asteroids are generally very similar to those of HEDs (Howardite–Eucrite–Diogenite meteorites) (McSween et al., 2013; Angrisani et al., 2023), which suggests that HEDs could have originated from Vesta and so they are representative of its expected mineralogy.

After Dawn arrival, VIR spectra of Vesta's surface confirmed the widespread presence of two absorption bands centered around 0.9 and 1.9 μm, confirming the widespread presence of iron-bearing low-calcium pyroxenes previously observed by telescopes (De Sanctis et al., 2013). These absorption bands are related to Fe^{2+} absorptions, while their band centers vary with pyroxene crystal chemistry: as the amount of Ca and/or Fe increases within the pyroxene structure, the positions of both bands shift toward longer wavelengths (Klima et al., 2007; Adams, 1974; Cloutis and et Gaffey, 1991). Thus, the spectral positions of these bands were used to infer the mineralogical composition of pyroxenes on

* Corresponding author at: INAF Istituto di Astrofisica e Planetologia Spaziali, via Fosso del Cavaliere, Rome 00133, Italy.
E-mail address: giuseppe.massa@inaf.it (G. Massa).

https://doi.org/10.1016/j.icarus.2023.115870
Received 27 July 2023; Received in revised form 5 November 2023; Accepted 12 November 2023
Available online 15 November 2023

Vesta's surface (De Sanctis et al., 2012a; De Sanctis et al., 2013).

Olivine was also used to characterize Vesta and its evolution (Ammannito et al., 2013). Evolutionary models of Vesta, generally used to infer its mineralogy, suggested a possible presence of olivine on the surface or in the mantle (Righter and et Drake, 1997; Ruzicka et al., 1997; Barrat et al., 2010; Mittlefehldt, 2000). Olivine was found in different areas with respect to what was suggested by models, suggesting an evolutionary history more complicated than previously thought (Ammannito et al., 2013; Palomba et al., 2015).

A fundamental vibrational absorption band at 2.8 μm due to the presence of hydroxyl on Vesta is present in VIR data for some areas, but its surface distribution is uneven (De Sanctis et al., 2012a, 2012b). The main candidate to be the cause of the presence of hydroxyl are hydroxyl-bearing impactors; this suggests that hydroxyl signatures might be associated with exogenous hydroxyl bearing carbonaceous chondrites, which are common in the main belt (McCord et al., 2012; Palomba et al., 2014). Recently, thanks to newly calibrated VIR data, every dark unit on Vesta was shown to be characterized by the presence of hydroxyl signatures, ruling out other possible causes of its presence (Massa et al., 2023).

In order to exclude shadows, a relative definition was adopted to identify a dark unit, i.e., a region darker and hotter than the surroundings. This definition allowed to find dark units even in brighter regions. The dark areas catalogue in Palomba et al. (2014) was built by dividing the areas into two main groups: Very Dark and Dark, with a reflectance value at 1.2 μm that is 30% or 15% lower, respectively, than the image average reflectance.

2. Dataset description and calibration

2.1. VIR spectrometer

The VIR spectrometer is derived from the VIRTIS-M on board ESA's Rosetta (Coradine et al., 1998) and Venus Express missions (Drossart et al., 2007). VIR mapping spectrometer acquires data in two spectral channels: the VIS channel operates from 0.25 to 1.05 μm and the IR channel from 1.0 to 5.0 μm. The high spatial (IFOV = 250 μrad/pixel, FOV = 64 × 64 mrad) and spectral ($\Delta\lambda_{VIS}$ = 1.8 nm/band; $\Delta\lambda_{IR}$ = 9.8 nm/band) performances allowed identification and mapping of the surface components and characteristics of Vesta, such as localized dark areas and the possible presence of localized exogenous materials (De Sanctis et al., 2011). VIR data have recently been newly calibrated with an improved S/N that allowed us to search for possible signatures that were dominated by the noise in the previous calibration (e.g., Massa et al., 2023). In Table 1, the orbital altitude, spatial resolution, and other details of Dawn mission observations at Vesta are reported. In the following, we used only data from the Hamo and Hamo-2 phases because they have a better compromise between spatial resolution and coverage of Vesta surface and because of the similar spatial resolution in these two phases.

2.2. Data calibration

After the radiometric and spectral calibration, a denoising algorithm (Carrozzo et al., 2016) was applied in order to remove the residual artifacts in VIR data. This algorithm was divided into five steps:

1. Selection of a portion of VIR spectra where no absorptions were present;
2. Computation of median spectra that characterized systematic residuals for each sample of the cube;
3. Application of a polynomial fitting to each median spectrum;
4. Definition of the artifact profiles as $(\textit{median spectrum of the sample} - \textit{fit of the spectrum}) / \textit{fit of the spectrum}$;
5. Removal of the column-dependent artifacts from the reflectance values applying the artifacts profile to the VIR reflectance spectra for each line.

Using this procedure, it was possible to remove the high frequency variations.

Moreover, a ground correction had to be applied to correct for fictitious slopes on both VIR channels (Raponi et al., 2020). To perform the ground correction, it was necessary to obtain ground observations of Vesta and then calculate the ratio between the smooth averaged spectrum of the ground-based spectra and the average spectrum of VIR-IR calibrated data after artifact correction. This ratio spectrum was used as a multiplicative correction factor on every single VIR spectrum.

Data acquired at Vesta by the visible channel of VIR is affected by the temperature of the visible sensor. The variations of the visible channel temperatures measured during the sessions of acquisitions were correlated with the variations in the spectral slope and shape for all the mission phases. An empirical correction based on a reference spectrum for the whole dataset was developed and applied (Rousseau, 2019). Moreover, the thermal emission of Vesta was also removed from the data (Raponi et al., 2019).

2.3. Vesta VIR IR spectra

The mean spectrum of about four hundred Vesta VIR IR spectra is shown in Fig. 1. In this spectrum, an absorption band around 1.9 μm is present due to the presence of pyroxenes, which was largely studied in De Sanctis et al., 2012a, 2013. Another band is present around 2.8 μm and is due to the presence of hydroxyl-bearing minerals (De Sanctis et al., 2012a, 2012b). This work was possible thanks to the new data calibration with an improved S/N of the spectra above 3 μm. In particular, a feature around 3.9 μm can be seen in Fig. 1 after a visual inspection of the spectrum. Finally, above 4 μm, the Vesta VIR IR spectra are noise-dominated.

3. Search for carbonates spectral signatures

Carbonaceous chondrites commonly contain carbonates (Doyle et al., 2015; de Leuw et al., 2010; Alexander et al., 2015). Carbonates show diagnostic vibrational absorption bands. There are six fundamental vibrational modes of the planar CO_3^{-2} ion, but since two of them are degenerate, there are only four different fundamental frequencies (Clark and Rencz, 1999; Hunt, 1977; Clark and Rencz, 1999; Hunt, 1977) that occur above 4 μm. In this section, the 4 μm combination mode (Nuevo et al., 2014; Palomba et al., 2016; Miyamoto and et Zolensky, 1994) will be searched in order to characterize the type of carbonaceous chondrites that can be present on Vesta. An overtone absorption band at 3.4 μm is present, but it is not visually seen in the spectra, so this band will be studied with a different approach in the next section (Clark and Rencz, 1999; Hunt, 1977; Palomba et al., 2016; Nuevo et al., 2014). In Fig. 2, four CM carbonaceous chondrites spectra taken from RELAB[1] database are shown, in which the 3.4 and 4 μm absorption bands are visible.

Table 1
Observation parameters of the orbital phases.

Phase	Altitude (km)	Lat (°)	Pixel Resolution (km)
Approach	2707–5497	70.0S-59.2N	0.677–1.374
Survey	2704–2874	90.0S-44.6N	0.676–0.719
HAMO	660–820	82.9S-45.8N	0.165–0.205
LAMO	172–298	90.0S-26.1N	0.043–0.075
HAMO-2	644–825	80.9S-70.7N	0.161–0.206

[1] RELAB is a spectral database that provides high quality spectroscopy data of minerals and mixtures.

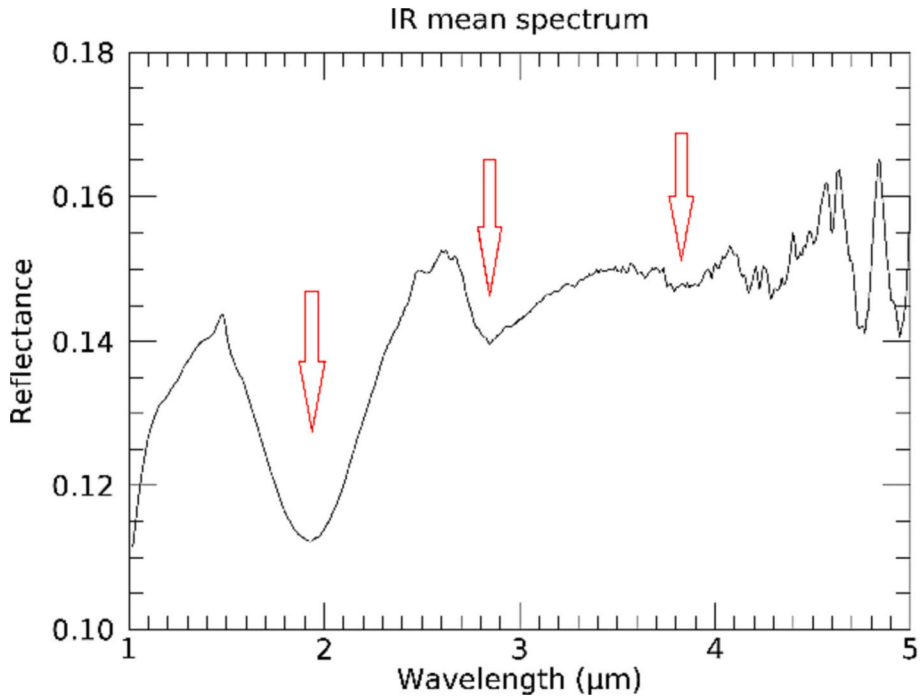

Fig. 1. IR mean spectrum.

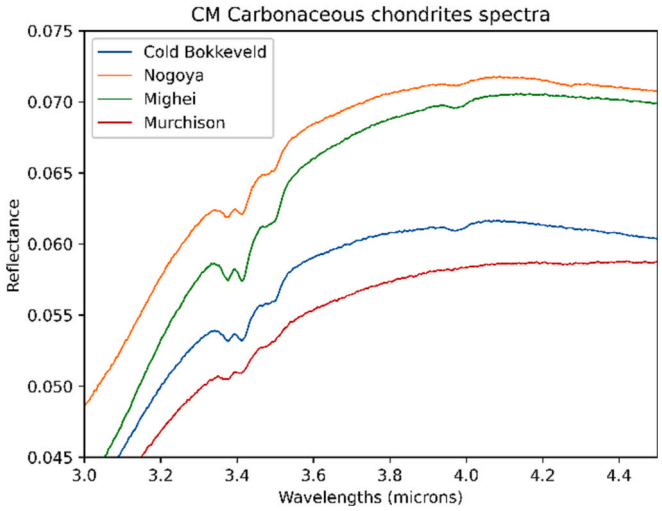

Fig. 2. CM carbonaceous chondrites spectra taken from RELAB database.

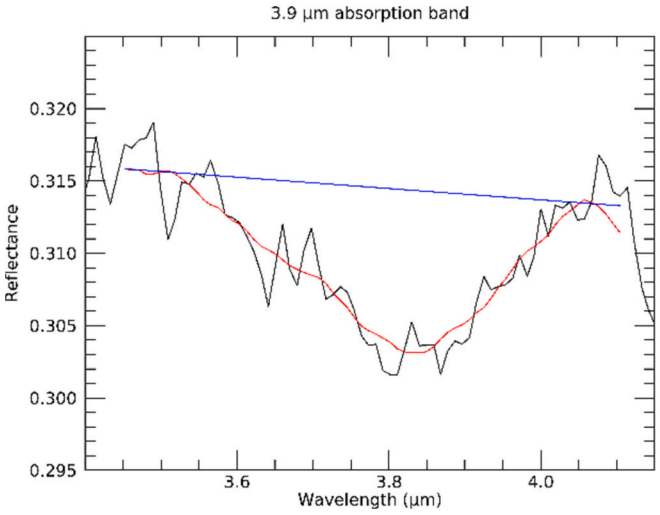

Fig. 3. 3.9 μm absorption band (red line) and its continuum (blue line). (For interpretation of the references to colour in this figure legend, the reader is referred to the web version of this article.)

To study the anti-correlation between the 3.9 μm feature and the reflectance, a procedure to calculate the band depth of the possible absorption band was defined based on the definition of the same bands adopted by Palomba et al. (2019). The spectra between 3.45 and 4.1 μm were smoothed, then the left shoulder of the absorption band was selected between 3.45 and 3.7 μm and the right one between 3.95 and 4.1 μm. To calculate the band depth, the continuum was removed from the absorption band. The continuum is the "background absorption" onto which other absorption features are superimposed (Clark and Roush, 1984; Clark and Rencz, 1999). In general, an absorption band may be located in the shoulder of a bigger absorption;, this will cause a sloping continuum, which in turn causes an apparent shift in the reflectance minimum and a change in the depth of the absorption band. The continuum was defined as the line between the local maximum of the shoulders of the absorption band (Fig. 3), and then it was removed from the absorption band.

3.1. Search for a possible relation between the 3.9 μm feature and the reflectance

Dark units are due to carbonaceous chondrites, and reflectance is anticorrelated with the hydroxyl absorption band at 2.8 μm (De Sanctis et al., 2012a, 2012b; Palomba et al., 2014; Massa et al., 2023). Based on this, if the feature at 3.9 μm is due to carbonates included in carbonaceous chondrites, it is expected to anticorrelate with the reflectance of Vesta surface.

To calculate the band depth, the position of the band center of the absorption band is needed, and it is defined as the location of the reflectance minimum inside the band after the continuum removal.

Now, the band depth can be calculated through the following relation (Clark and Roush, 1984):

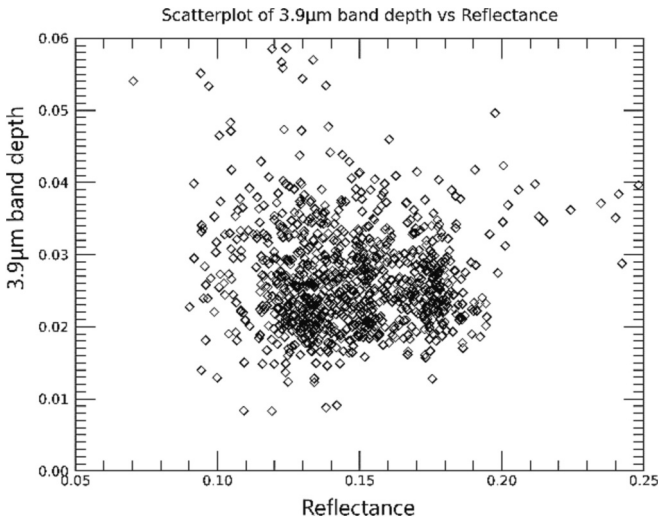

Fig. 4. Scatterplot between 3.9 μm band depth and 1.2 μm reflectance of the pixels of all the very dark units of Vesta taken from the catalogue in Palomba et al. (2014).

$$BD = 1 - \frac{R_c}{R_{con}}$$

where R_c and R_{con} are the measured reflectance and the calculated continuum reflectance at the band center, respectively.

In order to evaluate the possible relation between the 3.9 μm band depth and the reflectance level, a photometric correction had to be applied with respect to a possible dependence from the emission, phase, and radiation incidence angle. The carbonate 3.9 μm band is known to be independent of geometry (Longobardo et al., 2019). In addition, this was again verified in this work. Contrarily, the 1.2 μm reflectance was corrected adopting the empirical relation obtained in Longobardo et al. (2014).

No correlation is visible between the two variables (Fig. 4); this means that the feature at 3.9 μm is not related to the dark areas on Vesta.

3.2. Search for a possible relation between the 3.9 μm feature and the hydroxyl signature

The known relation between the hydroxyl and the reflectance on Vesta (De Sanctis et al., 2012a, 2012b) leads to the suggestion that carbonaceous chondrites could have been the carriers of hydroxyl-bearing molecules on Vesta surface. Therefore, even if the 3.9 μm feature, as shown in the previous paragraph, is not related to the dark areas, it can still be linked to the presence of hydroxyl. To search for a possible relation between the 3.9 μm feature and hydroxyl absorption band depth at around 2.8 μm, the latter was defined following the same procedure described above for the 3.9 μm band:

- The spectra were smoothed between 2.5 and 3.5 μm with a boxcar of nine VIR spectral bands.
- The left shoulder was selected from 2.5 to 2.75 μm, the right shoulder from 3 to 3.5 μm and the band trough from 2.75 to 3 μm.
- The continuum is defined as the linear fit between the shoulders maximum (
- Fig. 5).
- Finally, the continuum was removed from the band in order to find the band center that allowed the calculation of the band depth (Clark and Roush, 1984).

No photometrical correction was needed for the hydroxyl absorption band at 2.8 μm since it showed a slight, but negligible, dependence from the observation angles.

In Fig. 6 no correlation between the 3.9 μm feature and the hydroxyl absorption band is observed. This excludes the possibility that the feature at 3.9 μm may be due to the presence of carbonates.

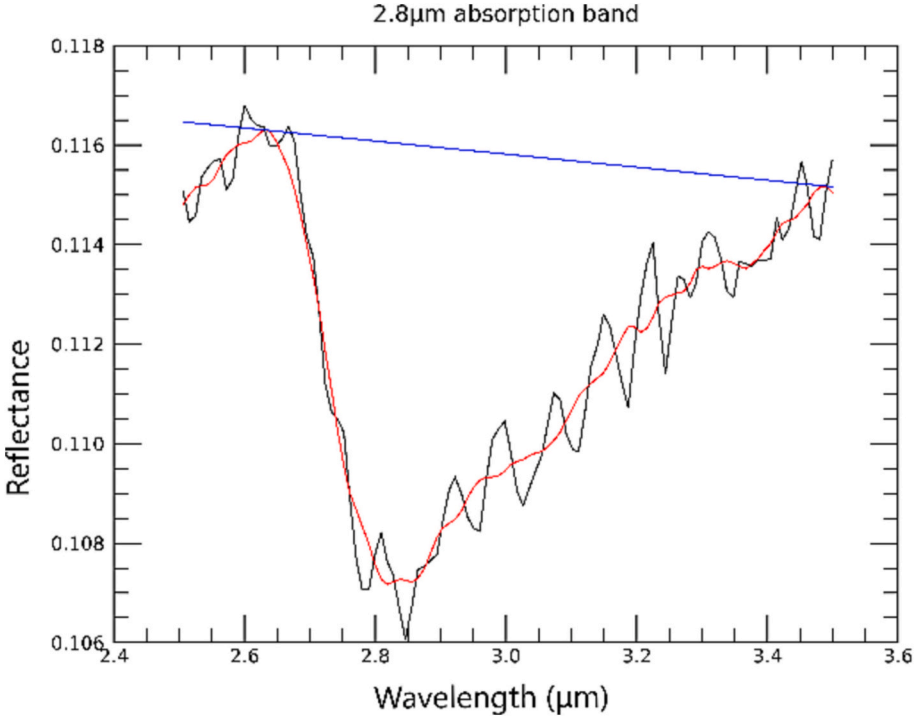

Fig. 5. Smoothing of the 2.8 μm absorption band (in red) and its superimposed continuum (in blue). (For interpretation of the references to colour in this figure legend, the reader is referred to the web version of this article.)

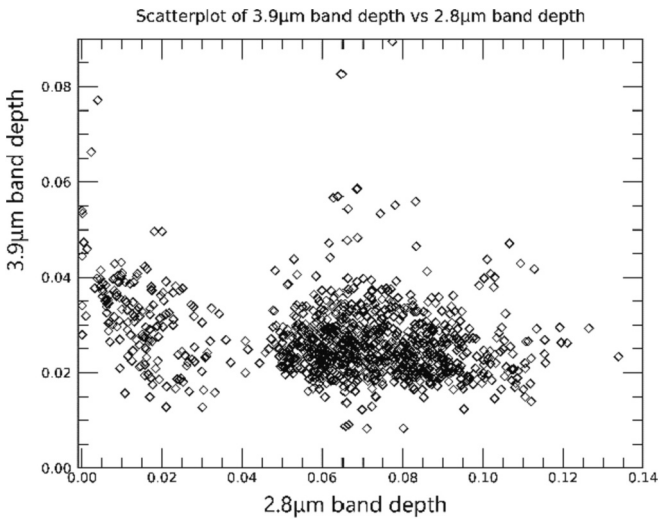

Fig. 6. Scatterplot between 3.9 μm band depth and 2.8 μm band depth.

3.3. Distribution of the 3.9 μm spectral feature

Although the 3.9 μm feature is not due to the presence of carbonaceous chondrites, it is indeed present in Vesta spectra. To understand its nature, its distribution across the entire Vesta surface (not only in dark units) was studied. The single datacube mean spectrum of about 250 brightest pixels is shown in Fig. 7. The feature at 3.9 μm can be clearly identified.

Since carbonates, and their features, are expected to be present only in dark units, the occurrence of this feature in bright units also excludes the possibility that it may be ascribed to the presence of carbonates. Nevertheless, it may still be due to a different, unidentified mineral, widespread on Vesta surface.

3.4. Classification of the 3.9 μm spectral feature as an artifact

Considering that Vesta spectra above 4 μm are dominated by residual noise due to thermal contribution removal, the chance that the 3.9 μm feature could be a spectral artifact was investigated.

A Noise Factor (NF) was defined as the normalized peak-to-peak difference in the spectral region between 4.75 and 5, where a noise induced artifact was present. This was just one of the possibilities for quantifying the noise. The scatterplot between 3.9 μm and NF is shown in Fig. 8. The two parameters are moderately correlated, as indicated by the Pearson coefficient of 0.4. The linear regression (red line) that shows the correlation between the band depth and the noise is shown in Fig. 8. This result suggests that the 3.9 μm feature is a noise-induced feature.

4. Study of the 3.4 μm absorption band

The absorption band at around 3.4 μm (Palomba et al., 2016; Hunt, 1977; Clark and Rencz, 1999; Nuevo et al., 2014) is also representative of carbonates. An extensive analysis of all the dark unit spectra did not reveal the 3.4 μm absorption band in any spectrum. The upper limit of the 3.4 μm band depth was calculated based on the VIR spectral noise, i.e., the minimum depth that the band should have in order to be observed. Thus, a procedure based on two steps was defined, i.e., 1) spectral noise assessment and 2) production of synthetic spectra and comparison with VIR spectra. This allowed us to estimate the upper limit of carbonaceous chondrites abundance.

4.1. Spectral noise evaluation

VIR spectral noise around 3.4 μm was evaluated by considering the average spectrum of every very dark unit, listed in Palomba et al. (2014). To produce the average spectrum, only the very dark units were considered because it is where the presence of carbonates, hence the depth of the 3.4 μm band, should be higher. Unreliable and very noisy spectra (i.e., spectral bands not observable) were excluded from the average. The mean spectrum was smoothed with a boxcar of 19 VIR spectral bands, and the obtained spectrum was defined as an "ideal signal" (i.e., noiseless, Fig. 9).

The noise was calculated in the range 3.25–3.6 μm as the root of the mean squared error (RMSE) relative to the mean reflectance of the smoothed spectra in the same interval of wavelengths with the following relation:

$$NOISE = \frac{\sqrt{\frac{\sum_{i=1}^{N}\left(x_i^{'}-x_i\right)^2}{N}}}{\frac{\sum_{i=1}^{N}x_i^{'}}{N}}$$

where $x_i^{'}$ and x_i are the reflectances of the ideal spectrum and the non-smoothed spectrum, respectively. Applying this relation, the noise value was found to be $2.2*10^{-3}$, hence all the spectral features having a depth lower than this value cannot be observed in the VIR spectra.

4.2. Synthetic spectra

In order to produce synthetic spectra of Vesta, a Radiative Transfer Model (RTM) was used, specifically the Hapke one that has been used for compositional analyses of planetary bodies (Hapke, 2012)(Hapke, 2012). The equation of radiative transfer describes the interactions of the radiation with the medium. To our ends, the bidirectional reflectance theory was used, which describes the radiation emitted by atmosphereless bodies. When modeling, scattering is very often considered to be isotropic, and this led to a simplification of the theory. To compute the analytical spectra, no opposition effect is considered because the RELAB spectra, from which the endmembers were taken to produce the synthetic spectra of Vesta, are taken at phase angles of 30°, where the opposition effect is negligible.

The whole procedure to compute the synthetic spectra can be schematized as follows:

1. Selection of mineral spectra that can be used as endmembers to reproduce the Vesta spectra: the spectra were built by combining the HED spectra (in turn obtained as a mixture of plagioclase and pyroxenes) with the Murchison carbonaceous chondrite (CM2) and with varying abundances of dolomite (from 0.02% to 0.7%). Dolomite is an anhydrous carbonate mineral composed of calcium magnesium carbonate, frequently found in carbonaceous chondrites (de Leuw et al., 2010).
2. Computation of the optical constants of these minerals with the tool in (Roush, 2005). Roush's tool is divided into two steps. The first one retrieves the dependence of extinction coefficient k with wavelength for a given spectrum, grain size, and the real part of the index of refraction n (all three given as input). The second one uses the Kramers-Kroning[2] relations to introduce the wavelength dependence of n index by taking the output file of the first procedure as an input. Since the analyzed spectra are in the near-infrared wavelength region, where the n index is weakly variable, it was assumed to be constant, avoiding the use of the second step.
3. Creation of single scattering albedo spectra at the fixed Vesta's grain size (Palomba et al., 2014) by using the optical constants spectra of minerals and Hapke's equation (Hapke, 2012).

[2] The Kramers-Kroning relations connect the real and imaginary parts of any complex function, that in this case is the refractive index.

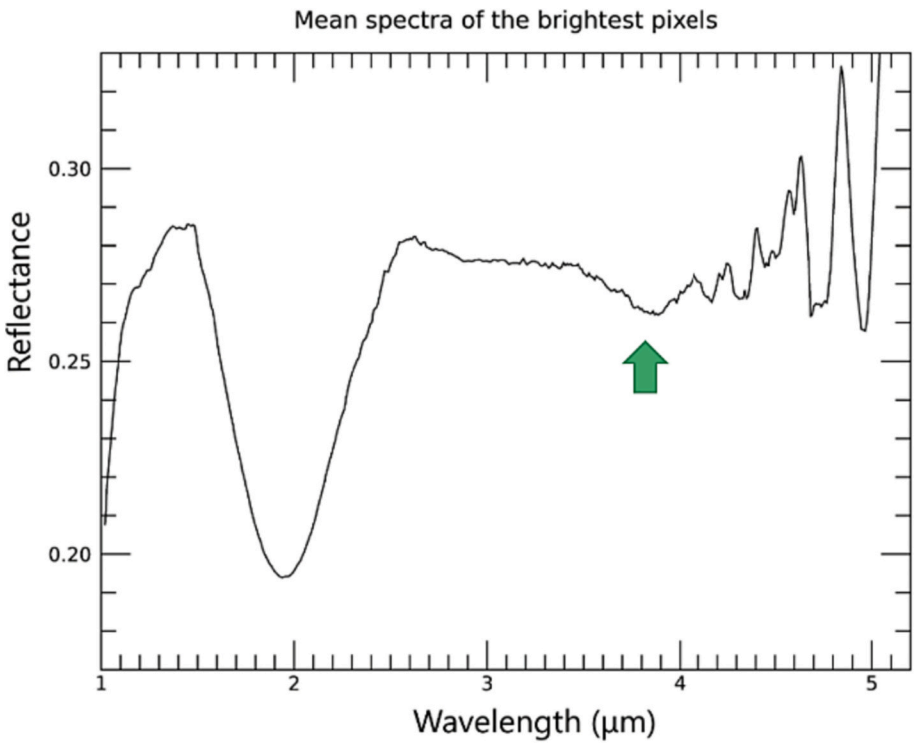

Fig. 7. Mean spectrum of the brightest pixels inside a datacube.

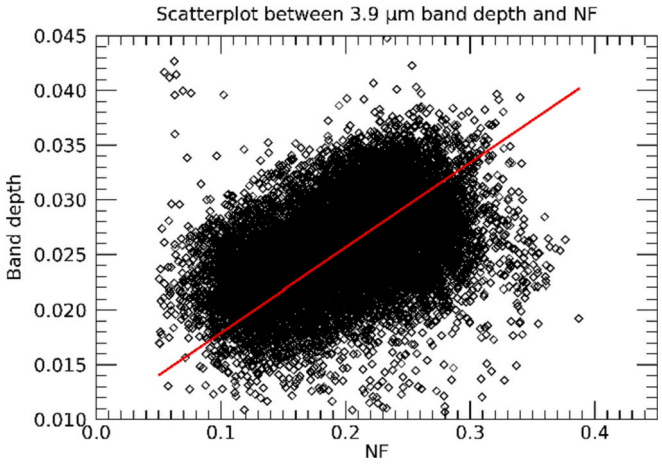

Fig. 8. Scatterplot between 3.9 μm band depth and NF of every pixel contained in a random datacube.

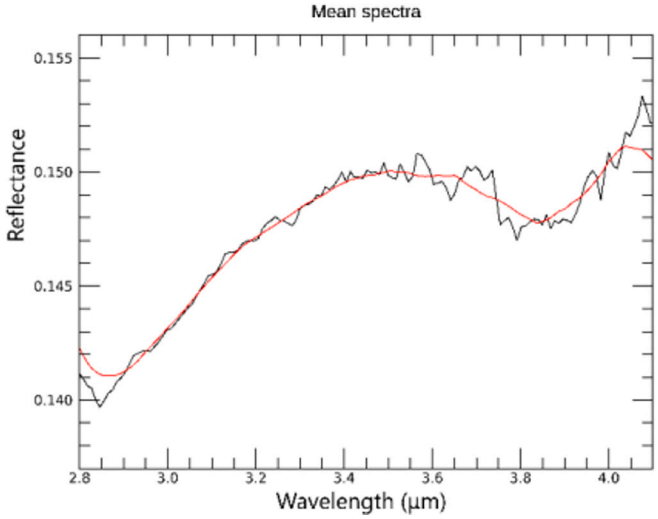

Fig. 9. Red) Mean spectra of dark regions on Vesta. Black) Smoothed spectra. (For interpretation of the references to colour in this figure legend, the reader is referred to the web version of this article.)

4. Generation of reflectance spectra using Hapke's equation to mix the single scattering albedos from different minerals.

In order to avoid carbonate band overestimation, the related Murchison carbonates band was removed from the spectra so that the only contribution to the 3.4 μm absorption band was due to the dolomite endmember.

Thirty-five spectra with four different abundances of CM2 (i.e., 20%, 30%, 40%, and 50%) were produced; those abundances of carbonaceous chondrites were chosen according to the estimation of 10–30% made by Palomba et al. (2014). The grain size was fixed at 35 μm in line with the estimated Vesta grain size, i.e., 0–45 μm (Palomba et al., 2014).

The 3.4 μm absorption band was studied, and its band depth was calculated on these spectra. In order to define the 3.4 μm band in these spectra, the shoulders were considered in the range of wavelength 3.25–3.3 μm for the left one and 3.5–3.58 μm for the right one, and then the continuum was computed as the line between the maxima of the two shoulders and removed from the spectra. Finally, the band depth was calculated. In Fig. 10, this absorption band appears as a doublet, but only the strongest absorption was studied.

4.3. Results and discussion

The noise value and the 3.4 μm band depth were compared in a scatterplot in order to estimate the upper limit to the abundance of carbonates (Fig. 11)

The 3.4 μm band depth variation with carbonates abundance can be

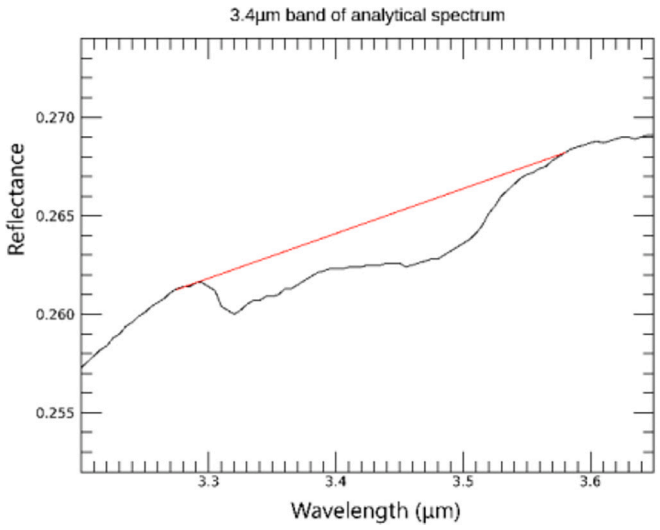

Fig. 10. *Black) 3.4* μm *absorption band; Red) Continuum line.* (For interpretation of the references to colour in this figure legend, the reader is referred to the web version of this article.)

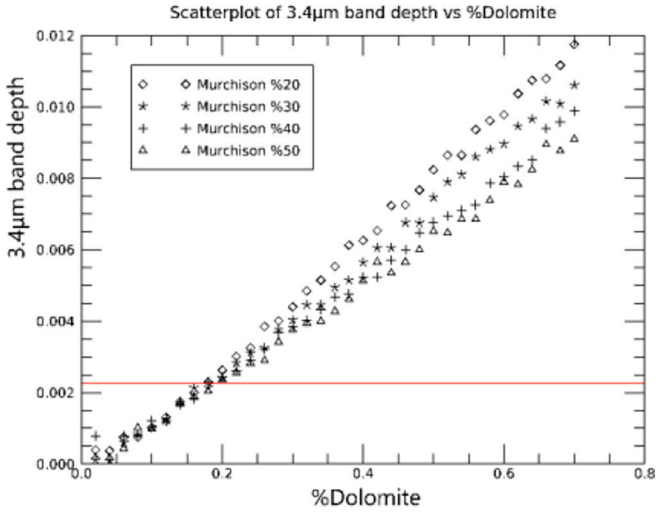

Fig. 11. Scatterplot between 3.4 μm band depth and abundance of carbonates in synthetical spectra.

observed, while the red line indicates the noise value (Fig. 11). It is worth noting that in the scatterplot for low dolomite amounts, the band depth is independent from the CM2 abundance, so the only contribution to the band depth is due to the abundance of carbonate. Since the 3.4 μm absorption band is not present in VIR spectra, this means that it is overwhelmed by the noise, so the value of the abundance of carbonates corresponding to the intersection between the noise value and the 3.4 μm band depth values is the upper limit to the carbonates abundance, because a larger value would allow observing the band. The estimated abundance of carbonates is around 0.18%.

The result was compared with the carbonate abundance found in CM carbonaceous chondrites (de Leuw et al., 2010) by petrochemical analyses. Indeed, it is thought that the carbonaceous chondrites on Vesta belong to the CM class (McCord et al., 2012). The following Table 2, taken from (de Leuw et al., 2010), shows that the carbonate abundances in CM chondrites span in the range 1–3%. Since the carbonaceous chondrites abundance on Vesta ranges from 10 to 30% (Palomba et al., 2014), the carbonates abundance should vary between 0.1 and 1%, therefore in good agreement with our estimations.

Table 2
Table of carbonates abundance in CM carbonaceous chondrites known in literature.

CM Chondrite	Modal abundance of carbonates
Y-791198	2.8 ± 0.6
LAP 04796	1.8 ± 0.3
Cold Bokkeveld	1.9 ± 0.2
Nogoya	1.4 ± 0.2
QUE 93005	2.3 ± 0.8
ALH 83100	2.8 ± 0.6
MET 01070	1.8 ± 0.8

5. Conclusions

In this work, the possible presence of carbonates on Vesta was investigated by studying their spectral signatures around 3.9 and 3.4 μm. The main reason behind the idea of the possible presence of carbonaceous chondrites on Vesta surface is that it was found that hydroxyl signatures showed an anticorrelation with reflectance, and the most accredited source of hydroxyl are exogenous carbonaceous chondrites.

The study of the 3.9 μm feature found that it is neither related to the dark areas on Vesta nor to the presence of hydroxyl signatures. This feature was found to correlate with a spectral artifact, leading to the conclusion that it is probably due to instrumental effects and not to something in the true Vesta spectrum, and its strength increases with increasing the noise level.

A visual inspection of the absorption band around 3.4 μm was inconclusive. In order to estimate an upper limit to the carbonate abundance, the following two-step procedure was followed:

1. Calculation of the noise around 3.4 μm;
2. Production of synthetic spectra representative of Vesta's expected mineralogy using a Radiative Transfer Model.

By comparing the obtained results, the upper limit to the carbonate abundance on Vesta's surface is found to be around 0.18%, in agreement with petrochemical analyses where the carbonates abundance should vary between 0.1 and 1% in a mixture containing an abundance of CCs from 10 to 30% as that supposed to be present on Vesta (Palomba et al., 2014).

In conclusion, this result is a first step to identify the carbonaceous chondrites that best reproduce those present on Vesta. We confirm that CM carbonaceous chondrites are likely mixed with HED, and some of them (e.g., LAP 04796, Cold Bokkeveld, Nogoya, MET 01070, QUE 93005) are fully consistent within uncertainty with our indications based on carbonate abundance.

Declaration of Competing Interest

The authors declare that they have no known competing financial interests or personal relationships that could have appeared to influence the work reported in this paper.

Data availability

VIR data of Vesta are available on the Planetary Data System (PDS) archive https://sbn.psi.edu/pds/resource/dawn/

References

Adams, J.B., 1974. Visible and Near-Infrared Diffuse Reflectance Spectra of Pyroxenes as Applied to Remote Sensing of Solid Objects in the Solar System, pp. 4829–4836. https://doi.org/10.1029/JB079i032p04829.
Alexander, C.O., et al., 2015. Carbonate abundances and isotopic compositions in chondrites, 50 (4), 810–833. https://doi.org/10.1111/maps.12410.

Alvarez-Candal, A., et al., 2006. The inner region of the asteroid Main Belt: a spectroscopic and dynamic analysis, 459.3, 969–976. https://doi.org/10.1051/0004-6361:20065518.
Ammannito, E., et al., 2013. Olivine in an unexpected location on Vesta's surface. Nature 504 (7478), 122–125. https://doi.org/10.1038/nature12665.
Angrisani, M., et al., 2023. A New Prospect to Analyse the Spectral Properties of v-Type Asteroids. https://doi.org/10.1016/j.icarus.2022.115320.
Barrat, J.-A., et al., 2010. Relative chronology of crust formation on asteroid Vesta: insights from the geochemistry of diogenites. Geochim. Cosmochim. Acta 74 (21), 6218–6231. https://doi.org/10.1016/j.gca.2010.07.028.
Carrozzo, F.G., et al., 2016. Artifacts Reduction in VIR/Dawn Data. https://doi.org/10.1063/1.4972256.
Clark, R.N., Rencz, A.N., 1999. Spectroscopy of Rocks and Minerals, and Principles of Spectroscopy.
Clark, R.N., Roush, T.L., 1984. Reflectance spectroscopy: quantitative analysis techniques for remote sensing applications. J. Geophys. Res. Solid Earth 89 (B7), 6329–6340. https://doi.org/10.1029/JB089iB07p06329.
Cloutis, E.A., et Gaffey, M.J., 1991. Pyroxene Spectroscopy Revisited: Spectral-Compositional Correlations and Relationship to Geothermometry, pp. 22809–22826. https://doi.org/10.1029/91JE02512.
Coradine, A., et al., 1998. VIRTIS: an imaging spectrometer for the Rosetta mission. Planet. Space Sci. 46 (9–10), 1291–1304. https://doi.org/10.1016/S0032-0633(98)00025-7.
de Leuw, S., Rubin, A.E., Wasson, J.T., 2010. Carbonates in CM chondrites: complex formational histories and comparison to carbonates in CI chondrites. Meteorit. Planet. Sci. 45 (4), 513–530. https://doi.org/10.1111/j.1945-5100.2010.01037.x.
De Sanctis, M.C., et al., 2011. The VIR spectrometer. In: The Dawn Mission to Minor Planets 4 Vesta and 1 Ceres. Springer, New York, NY, pp. 329–369. https://doi.org/10.1007/978-1-4614-4903-4_13.
De Sanctis, M.C., et al., 2012a. Detection of widespread hydrated materials on Vesta by the VIR imaging spectrometer on board the Dawn mission. Astrophys. J. Lett. 758 (2), L36. https://doi.org/10.1088/2041-8205/758/2/L36.
De Sanctis, M.C., et al., 2012b. Spectroscopic Characterization of Mineralogy and its Diversity Across Vesta, pp. 697–700. https://doi.org/10.1126/science.1219270.
De Sanctis, M.C., et al., 2013. Vesta's mineralogical composition as revealed by the visible and infrared spectrometer on Dawn. Meteorit. Planet. Sci. 48 (11), 2166–2184. https://doi.org/10.1111/maps.12138.
DeMeo, F.E., et al., 2009. An extension of the Bus asteroid taxonomy into the near-infrared, 202 (1), 160–180. https://doi.org/10.1016/j.icarus.2009.02.005.
Doyle, P.M., et al., 2015. Early Aqueous Activity on the Ordinary and Carbonaceous Chondrite Parent Bodies Recorded by Fayalite, p. 6.1. https://doi.org/10.1038/ncomms8444.
Drossart, P., et al., 2007. Scientific goals for the observation of Venus by VIRTIS on ESA/Venus express mission. Planet. Space Sci. 55 (12), 1653–1672. https://doi.org/10.1016/j.pss.2007.01.003.
Duffard, R., et al., 2004. Mineralogical characterization of some basaltic asteroids in the neighborhood of (4) Vesta: First results, 171 (1), 120–132. https://doi.org/10.1016/j.icarus.2004.05.004.
Hapke, B., 2012. Theory of Reflectance and Emittance Spectroscopy. Cambridge University Press. https://doi.org/10.1017/CBO9781139164344.
Hunt, G.R., 1977. Spectral signatures of particulate minerals in the visible and near infrared. Geophysics 42 (3), 501–513. https://doi.org/10.1190/1.1440721.
Klima, R.L., Pieters, C.M., Dyar, M.D., 2007. Spectroscopy of synthetic mg-Fe pyroxenes I: spin-allowed and spin-forbidden crystal field bands in the visible and near-infrared. Meteorit. Planet. Sci. 42 (2), 235–253. https://doi.org/10.1111/j.1945-5100.2007.tb00230.x.
Longobardo, A., et al., 2014. Photometric behavior of spectral parameters in Vesta dark and bright regions as inferred by the Dawn VIR spectrometer. Icarus 240, 20–35. https://doi.org/10.1016/j.icarus.2014.02.014.
Longobardo, A., et al., 2019. Photometry of Ceres and Occator faculae as inferred from VIR/Dawn data, 320, 97–109. https://doi.org/10.1016/j.icarus.2018.02.022.
Massa, G., et al., 2023. Pyroxene and Hydroxyl Signatures in Vesta Newly Calibrated Data from Dawn Mission. https://doi.org/10.3390/universe9060296.
McCord, T.B., et al., 2012. Dark material on Vesta from the infall of carbonaceous volatile-rich material. Nature 491 (7422), 83–86. https://doi.org/10.1038/nature11561.
McSween, J.H., et al., 2013. Dawn; the Vesta–HED connection; and the geologic context for eucrites, diogenites, and howardites. Meteorit. Planet. Sci. 48 (11), 2090–2104. https://doi.org/10.1111/maps.12108.
Mittlefehldt, D.W., 2000. Petrology and geochemistry of the elephant moraine A79002 diogenite: a genomict breccia containing a magnesian harzburgite component. Meteorit. Planet. Sci. 35 (5), 901–912. https://doi.org/10.1111/j.1945-5100.2000.tb01479.x.
Miyamoto, M., et Zolensky, M.E., 1994. Infrared Diffuse Reflectance Spectra of Carbonaceous Chondrites: Amount of Hydrous Minerals, pp. 849–853. https://doi.org/10.1111/j.1945-5100.1994.tb01098.
Nuevo, M., et al., 2014. Mid-infrared study of stones from the Sutter's Mill meteorite, 49 (11), 2017–2026. https://doi.org/10.1111/maps.12269.
Palomba, E., et al., 2014. Composition and mineralogy of dark material units on Vesta. Icarus 240, 58–72. https://doi.org/10.1016/j.icarus.2014.04.040.
Palomba, E., et al., 2015. Detection of new olivine-rich locations on Vesta. Icarus 258, 120–134. https://doi.org/10.1016/j.icarus.2015.06.011.
Palomba, E., et al., 2016. Characterization of carbonates on Ceres. In: 47th Annual Lunar and Planetary Science Conference. No. 1903.
Palomba, E., et al., 2019. Compositional differences among Bright Spots on the Ceres surface, 320, 202–212. https://doi.org/10.1016/j.icarus.2017.09.020.
Prettyman, T.H., et al., 2011. Dawn's gamma ray and neutron detector. In: The Dawn Mission to Minor Planets 4 Vesta and 1 Ceres. Springer, New York, NY, pp. 371–459. https://doi.org/10.1007/978-1-4614-4903-4_14.
Raponi, A., et al., 2019. Mineralogy of Occator Crater on Ceres and Insight into its Evolution from the Properties of Carbonates, Phyllosilicates, and Chlorides, pp. 83–96. https://doi.org/10.1016/j.icarus.2018.02.001.
Raponi, A., et al., 2020. Organic Material on Ceres: Insights from Visible and Infrared Space Observations. https://doi.org/10.3390/life11010009.
Righter, K., et Drake, M.J., 1997. A magma ocean on Vesta: Core formation and petrogenesis of eucrites and diogenites. Meteorit. Planet. Sci. 32 (6), 929–944. https://doi.org/10.1111/j.1945-5100.1997.tb01582.x.
Roush, T.L., 2005. Near-infrared (0.67–4.7 μm) optical constants estimated for montmorillonite. Icarus 179 (1), 259–264.
Rousseau, B., 2019. Correction of the VIR-Visible Data Set from the Dawn Mission. https://doi.org/10.1063/1.5123362.
Ruzicka, A., Snyder, G.A., Taylor, L.A., 1997. Vesta as the howardite, eucrite and diogenite parent body: implications for the size of a core and for large-scale differentiation. Meteorit. Planet. Sci. 32 (6), 825–840. https://doi.org/10.1111/j.1945-5100.1997.tb01573.x.
Sierks, H., et al., 2011. The Dawn framing camera. Space Sci. Rev. 163 (1), 263–327. https://doi.org/10.1007/s11214-011-9745-4.
Xu, S., et al., 1995. Small main-belt asteroid spectroscopic survey: Initial results, 115 (1), 1–35. https://doi.org/10.1006/icar.1995.1075.